Characteristics of Epitaxial Graphene on SiC/Si Substrates in the Radio Frequency Spectrum

David A. Katzmarek, *Graduate Student Member, IEEE*, Yang Yang, *Senior Member, IEEE*, Mohammad B. Ghasemian, Kourosh Kalantar-Zadeh, *Senior Member, IEEE*, Richard W. Ziolkowski, *Life Fellow, IEEE*, and Francesca Iacopi, *Senior Member, IEEE*

***Abstract*— Graphene is expected to bring substantial benefits for high-frequency applications, however, most of the studies in this area are based on theory. Here, the properties of epitaxial graphene grown on intrinsic silicon carbide on silicon substrates are investigated for potential radio frequency (RF) applications. Metal coplanar waveguides (CPWs) are fabricated that employ graphene as a shunt between the signal and ground planes. The CPWs are used for characterizing the frequency-dependent behavior of the sheet resistance of the graphene shunt from 10 MHz to 10 GHz. The process involves evaluating the CPW's RLCG transmission line parameters and comparing them to a reference un-shunted CPW to extract the sheet resistance. We find that the quality of the metal contact with graphene is one key parameter to observe adequate current injection in the 2D material in the RF spectrum. A mild argon plasma treatment was applied to reach an adequate contact quality. Furthermore, we observe a monotonic decrease of the sheet resistance of the epitaxial graphene for frequencies roughly above 100 MHz. We attribute this behavior to the progressively smaller influence of small-scale discontinuities, such as grain sizes, at those higher frequencies.**

***Index Terms*— Coplanar waveguides, contact resistance, graphene, radio frequency, sheet resistance.**

I. Introduction

EVER since graphene's exceptional transport properties were fully described by Novoselov et al. [1], the fabrication of graphene-based electronic devices has also been extensively investigated to utilize its remarkable properties in electronic devices [2]. Interactions between graphene and the substrate, on which it resides or other surrounding materials [2], as well as achieving an adequate electrical contact due to the high contact resistance at graphene-metal interfaces [3], [4], are some of the most prominent issues encountered when integrating graphene.

While a high contact resistance, although not ideal, would normally not impede the operation of a device at direct current (DC) operation, the impact of a high contact resistance in radio frequency (RF) applications has been shown to be quite significant [3], [4]. Graphene is expected to bring major benefits for RF to terahertz applications due to its high electrical conductivity, support of surface-plasmon-polaritons, and dynamic tunability [5]. While several publications have focused on the contact resistance of graphene, its effect has rarely been studied experimentally at RF frequencies. Furthermore, simulation models often assume an ideal contact resistance [5].

Epitaxial graphene (EG) grown on silicon carbide-on-silicon (SiC/Si) wafers using a catalytic alloy-mediated graphitization approach [6], [7] was employed for this study. DC electrical characterization of EG grown on intrinsic 3C-(111) SiC/Si has indicated sheet resistance in the range of 2.5 to 9 kΩ $\square^{-1}$, p-type sheet carrier concentrations of 3.3 to 7 $\times$ 10^{12} cm^{-2} with a mobility of 144 to 330 cm^2V^{-1} s^{-1}, and consists of 3 to 7 layers with grain sizes of $<$100 nm [8]. The Drude model for graphene predicts a constant conductivity up to the THz range. However, RF measurements have shown deviations from their corresponding DC conductivity measurements [9], [10].

II. Device Structure and Fabrication

Coplanar waveguides (CPWs) were used to characterize the sheet resistance of the graphene shunt. The main structure of the CPWs consisted of metal as it can be deposited as a relatively thick layer in comparison to the graphene. This improves the transmission properties of the CPW [11], [12]. The graphene is placed between the signal and GND planes of a metal CPW [13], as shown in Fig. 1.

The individual fabrication steps are illustrated in Fig. 2 and outlined in Table I. EG was grown on intrinsic 3C-(111) SiC/Si substrates using a catalytic alloy-mediated graphitization process [6], [7]. It was patterned by pre-structuring the metal catalyst using UV-lithography patterned photoresist (PR) and a lift-off technique.

Manuscript received 21 November 2022; revised 7 December 2022; accepted 14 December 2022. Date of publication 19 December 2022; date of current version 27 January 2023. This work was supported by the Australian Research Council through the Centre of Excellence in Transformative Meta-Optical Systems (TMOS) under Grant CE200100010. The review of this letter was arranged by Editor G. Han. *(Corresponding author: Francesca Iacopi.)*

David A. Katzmarek and Francesca Iacopi are with the ARC Centre of Excellence TMOS, Faculty of Engineering and IT, University of Technology Sydney, Sydney, NSW 2007, Australia (e-mail: francesca.iacopi@uts.edu.au).

Yang Yang is with the Faculty of Engineering and IT, University of Technology Sydney, Sydney, NSW 2007, Australia.

Mohammad B. Ghasemian is with the Faculty of Engineering, University of New South Wales, Sydney, NSW 2052, Australia.

Kourosh Kalantar-Zadeh is with the Faculty of Engineering, University of New South Wales, Sydney, NSW 2052, Australia, and also with the School of Chemical and Biomolecular Engineering, The University of Sydney, Sydney, NSW 2008, Australia.

Richard W. Ziolkowski is with the Faculty of Engineering and IT, University of Technology Sydney, Sydney, NSW 2007, Australia, and also with the Department of Electrical and Computer Engineering, University of Arizona, Tucson, AZ 85721 USA.

Color versions of one or more figures in this letter are available at https://doi.org/10.1109/LED.2022.3230358.

Digital Object Identifier 10.1109/LED.2022.3230358

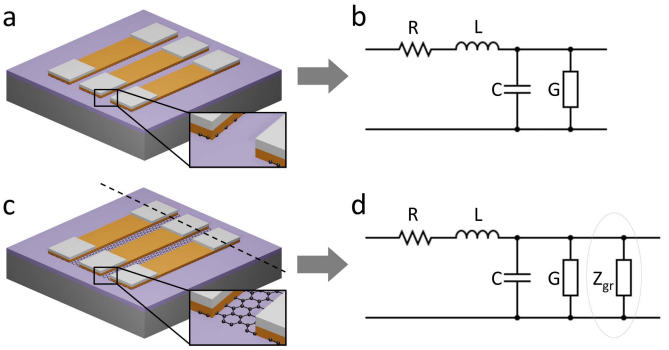

Fig. 1. (a) Illustration of a graphene un-shunted CPW on SiC/Si substrate. The inset shows that graphene is only underneath the metal CPW, not between the signal and ground (GND) planes. (b) RLCG model of the un-shunted CPW in (a). (c) Illustration of a graphene-shunted CPW. The dashed line visualizes the plane for the fabrication description in Fig. 2. The inset shows that the graphene lies in the gaps of and underneath the signal and GND planes and, hence, acts as a shunt. (d) RLCG model of the graphene shunted CPW in (c).

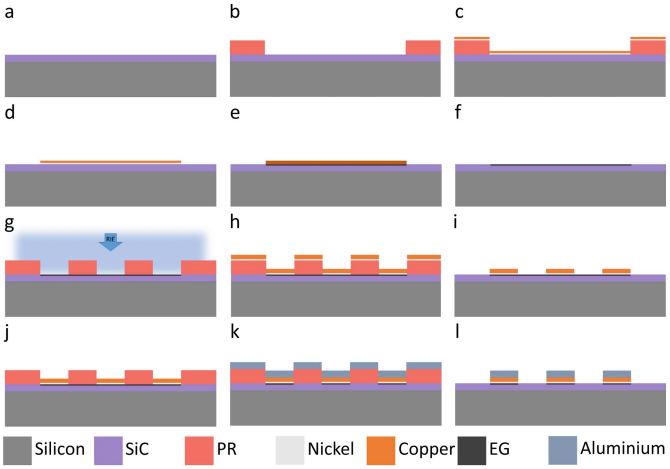

Fig. 2. Schematic illustration of the fabrication steps required to manufacture metal CPWs employing EG on SiC/Si substrates. EG is structured via the pre-structuring of the catalyst metals before graphitization. A description of individual steps is given in Table I.

TABLE I
DESCRIPTION OF FABRICATION STEPS FOR THE SCHEMATICS IN FIG 2

Step	Description
a	Bare SiC/Si intrinsic substrate
b	Patterning of PR via UV lithography for lift-off of metal catalysts
c	Deposition of Ni (10 nm) and Cu (20 nm) for graphitization
d	Lift-off using sonication in acetone
e	Graphitization via annealing at 1100°C for one hour
f	Freckle etch to remove metal catalysts and silicides
g	Patterning of PR via UV lithography for lift-off of metal CPW as well as O_2 de-scum and Ar treatment via ICP-RIE
h	Deposition of Ni (5 nm) and Cu (100 nm) to form the CPW structure
i	Lift-off using sonication in acetone
j	Patterning of PR via UV lithography for lift-off of Al contact pads
k	Deposition of Al contacts
l	Lift-off using sonication in acetone

Two samples were fabricated using two separate substrates. Each contains three sets of un-shunted and shunted CPWs. The CPWs have the following dimensions: their total length and width are 350 μm and 250 μm, respectively; the width

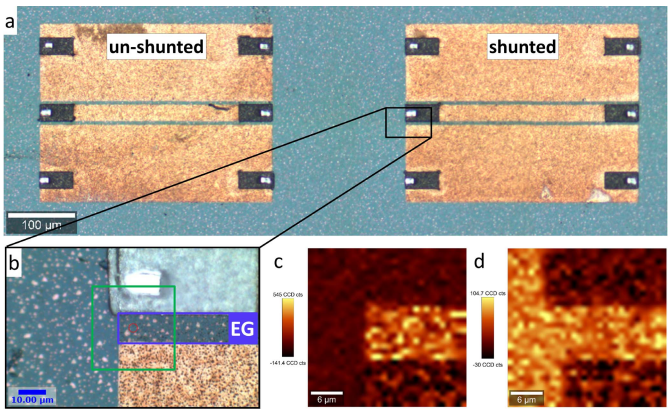

Fig. 3. (a) Structures of (left) regular CPW and (right) graphene-shunted CPW. (b) Microscope image of the Raman mapping area (green square) showing the bare SiC substrate on the left, the Al pad on the top-right, and the Cu CPW on the bottom-right, with the graphene shunt in between (blue square). (c-d) Raman intensity maps of (c) graphene's 2D (~2700 cm^{-1}) and (d) the SiC LO (~970 cm^{-1}) peaks.

of the center trace is 25 μm; the gap width is 5 μm; and the pad dimensions are 25 μm × 50 μm. The final fabricated structures can be seen in Fig. 3. The magnified view of the gap between the signal and the GND planes of a shunted CPW shows the graphene area. Raman large area mapping (30 μm × 30 μm) spectroscopy was used to identify the graphene shunt and confirm that it is only located in the gap.

During the fabrication process, we experienced significant difficulties with the adhesion of the metal CPW to the graphene. Lifting off the contact pads would invariably result in a complete or partial delamination of the CPW structures. A brief oxygen (O_2) plasma de-scum treatment (5 s, P_{ICP} = 10 W, P_{RIE} = 30 W, 10 mT, O_2: 12 sccm) using inductively coupled plasma reactive ion etching (ICP-RIE) was introduced to mitigate the poor adhesion, attributed to photoresist residues.

Furthermore, a mild Ar plasma treatment of the graphene-metal contact area using ICP-RIE was introduced (60 s, P_{ICP} = 50 W, P_{RIE} = 30W, 20 mT, Ar: 20 sccm) to create defects in the graphene for an increased extent of edge contact with the metal, hence reducing the contact resistance [14].

III. DISCUSSION

Large-area Raman maps (four per sample, 30 μm × 30 μm, 30 × 30 points) were used to characterize the graphene of the two samples before any treatment was performed. The I_D/I_G and I_{2D}/I_G ratios were I_D/I_G = 0.34 (±0.01) and I_{2D}/I_G = 1.17 (±0.08), as well as I_D/I_G = 0.35 (±0.02) and I_{2D}/I_G = 1.16 (±0.08). They are in line with previously reported values [8].

A comparison of the S-parameters of the shunted and un-shunted CPW structures on the samples where the graphene-metal contact areas were either exposed or not exposed to the Ar treatment is shown in Fig. 4. While the untreated CPWs show no difference between the shunted and un-shunted CPWs, with $|S_{11,1GHz}|$ and $|S_{21,1GHz}|$ remaining constant at about −27.4 dB and −0.8 dB, respectively, the treated ones show a significant difference. $|S_{11,1GHz}|$ increases from −25.18 (±0.14) dB to −21.79 (±0.51) dB and $|S_{21,1GHz}|$

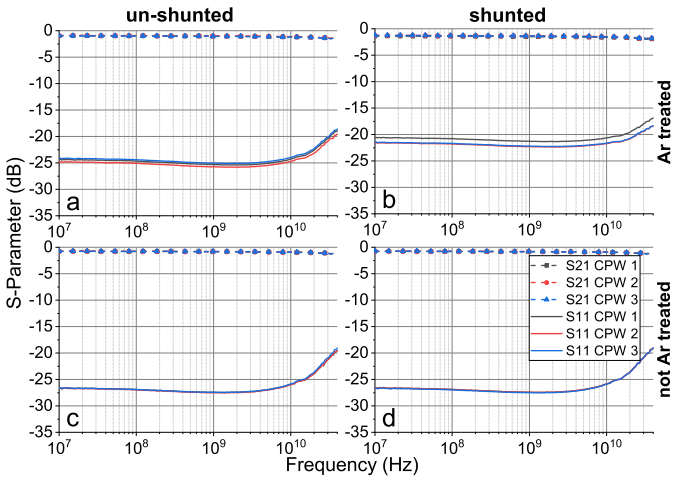

Fig. 4. Comparison of the S-parameters of CPWs where (a,b) the graphene at the metal contacts were Ar-treated (ICP-RIE) before metal deposition and (c,d) the graphene was not exposed to Ar plasma. (Legend in (d) applies to all graphs).

decreases from −1.01 (±0.04) dB to −1.41 (±0.07) dB. These characteristics arise from the improved contact to the underlying graphene, resulting in the graphene shunt shorting the signal and GND planes of the CPWs. Indeed, placing the graphene shunt in the CPW structure results in higher reflections due to a mismatch of the characteristic impedance of the CPW to the RF probe and a consequent increase in $|S_{11}|$ and a decrease in $|S_{21}|$.

In contrast, there is a minor difference in the $|S_{11,1GHz}|$ and $|S_{21,1GHz}|$ of the un-shunted CPWs of the two samples (∼1.8 dB and ∼0.2 dB, respectively) as illustrated in Fig. 4. (a) and (c), that we attribute to sample-to-sample dimensions variability of the CPWs, due to the individual UV lithography processing on each sample.

The graphene shunt's frequency-dependent sheet resistance is evaluated by extracting the RLCG parameters [15] of the shunted and reference un-shunted CPWs that otherwise have the same dimensions. It can be assumed that the insertion of a graphene shunt, as illustrated in Fig. 1, will only influence the G parameter of the shunted CPW, as graphene's Drude conductivity model predicts a purely real conductivity in this frequency band. The sheet resistance simply becomes:

$$G_{Gr,shunt} = G_{shunted} - G_{un-shunted} \quad (1)$$

$$R_{s,Gr} = \frac{w}{2lG_{Gr,shunt}} \quad (2)$$

with $G_{shunted}$ and $G_{un-shunted}$ being the extracted G parameters of the CPWs and w and l being their gap width and length, respectively.

The epitaxial graphene employed in this study has a relatively high charge carrier concentration of 3.3 to 7×10^{12} cm^{-2} [8], which typically tends to deliver a lower contact resistance [3]. However, surface roughness has a detrimental effect on the contact resistance [16], [17], and this EG on 3C-(111) SiC/Si has an inherent root mean square roughness of ∼9 nm [7]. Using transfer length method (TLM) structures, we have evaluated an initial contact resistance of

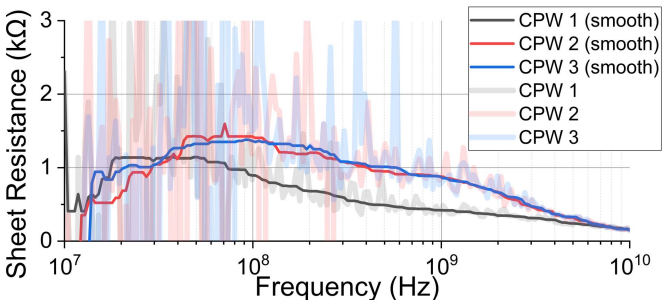

Fig. 5. Extracted sheet resistance of the EG shunts of three shunted CPWs on the Ar-treated sample.

∼2.9 MΩμm. Nevertheless, the mild Ar treatment, bringing the contact resistance down to a value of <2.7 MΩμm, was necessary to ensure optimal coupling.

Fig. 5 plots the extracted sheet resistance of three shunted CPWs. Between 10 MHz and 80 MHz, the measurement data is very noisy and does not allow for reliable data extraction. This could potentially be mitigated using longer CPW structures. Between 80 MHz and 1 GHz, the extraction of the sheet resistance is relatively steady and shows a monotonic decline of the sheet resistance starting above/around ∼100 MHz from 1.5 kΩ (value in line with the DC measurements [8]) down to 0.9 kΩ for CPW 1 and CPW 2 and from 0.9 kΩ down to 0.5 kΩ for CPW 3. We attribute this effect to the decrease of the influence of grain-boundary scattering on the sheet resistance of the graphene. We recall that the EG has grain sizes of <100 nm in size [8] in comparison to an EM field wavelength of about 3 m at 100 MHz. Therefore, the small-scale defects within the graphene layer that play a significant role in DC measurements tend to show less influence in the RF measurements [10], [18].

Further, CPW 3, which has the lowest sheet resistance, has the highest $|S_{11}|$, see Fig. 4 (b), which is attributed to the increased reflection due to the low resistance shunt.

IV. Conclusion

This work shows the RF characteristics of epitaxial graphene grown on SiC/Si substrates using a catalytic alloy-mediated graphitization process. We affirm the importance of achieving a sufficiently low graphene-metal contact resistance for adequate current injection in the 2D material at high frequencies. We also observe a strong frequency dependence of graphene's sheet resistance. This is attributed to the increasingly lower influence of small-scale scattering defects in the graphene at high frequencies, such as the <100 nm grain sizes.

Acknowledgment

The authors acknowledge Lang Chen from the University of Technology Sydney for assistance with the probe measurements.

References

[1] K. S. Novoselov, A. K. Geim, S. V. Morozov, D. Jiang, Y. Zhang, S. V. Dubonos, I. V. Grigorieva, and A. A. Firsov, "Electric field effect in atomically thin carbon films," *Science*, vol. 306, no. 5696, pp. 666–669, Oct. 2004, doi: 10.1126/science.1102896.

[2] J. Yang, P. Hu, and G. Yu, "Perspective of graphene-based electronic devices: Graphene synthesis and diverse applications," *APL Mater.*, vol. 7, no. 2, Feb. 2019, Art. no. 020901, doi: 10.1063/1.5054823.

[3] L. Anzi, A. Mansouri, P. Pedrinazzi, E. Guerriero, M. Fiocco, A. Pesquera, A. Centeno, A. Zurutuza, A. Behnam, E. A. Carrion, E. Pop, and R. Sordan, "Ultra-low contact resistance in graphene devices at the dirac point," *2D Mater.*, vol. 5, no. 2, Feb. 2018, Art. no. 025014, doi: 10.1088/2053-1583/aaab96.

[4] A. Hsu, H. Wang, K. K. Kim, J. Kong, and T. Palacios, "Impact of graphene interface quality on contact resistance and RF device performance," *IEEE Electron Device Lett.*, vol. 32, no. 8, pp. 1008–1010, Aug. 2011, doi: 10.1109/LED.2011.2155024.

[5] D. A. Katzmarek, A. Pradeepkumar, R. W. Ziolkowski, and F. Iacopi, "Review of graphene for the generation, manipulation, and detection of electromagnetic fields from microwave to terahertz," *2D Mater.*, vol. 9, no. 2, Mar. 2022, Art. no. 022002, doi: 10.1088/2053-1583/ac59d1.

[6] N. Mishra, J. J. Boeckl, A. Tadich, R. T. Jones, P. J. Pigram, M. Edmonds, M. S. Fuhrer, B. M. Nichols, and F. Iacopi, "Solid source growth of graphene with Ni–Cu catalysts: Towards high qualityin situ-graphene on silicon," *J. Phys. D, Appl. Phys.*, vol. 50, no. 9, Feb. 2017, Art. no. 095302, doi: 10.1088/1361-6463/aa560b.

[7] F. Iacopi, N. Mishra, B. V. Cunning, D. Goding, S. Dimitrijev, R. Brock, R. H. Dauskardt, B. Wood, and J. Boeckl, "A catalytic alloy approach for graphene on epitaxial SiC on silicon wafers," *J. Mater. Res.*, vol. 30, no. 5, pp. 609–616, Mar. 2015, doi: 10.1557/jmr.2015.3.

[8] A. Pradeepkumar, M. Amjadipour, N. Mishra, C. Liu, M. S. Fuhrer, A. Bendavid, F. Isa, M. Zielinski, H. I. Sirikumara, T. Jayasekara, D. K. Gaskill, and F. Iacopi, "P-type epitaxial graphene on cubic silicon carbide on silicon for integrated silicon technologies," *ACS Appl. Nano Mater.*, vol. 3, no. 1, pp. 830–841, Dec. 2020, doi: 10.1021/acsanm.9b02349.

[9] N. Rouhi, S. Capdevila, D. Jain, K. Zand, Y. Y. Wang, E. Brown, L. Jofre, and P. Burke, "Terahertz graphene optics," *Nano Res.*, vol. 5, no. 10, pp. 667–678, Sep. 2012, doi: 10.1007/s12274-012-0251-0.

[10] J. L. Tomaino, A. D. Jameson, J. W. Kevek, M. J. Paul, A. M. Van Der Zande, R. A. Barton, P. L. McEuen, E. D. Minot, and Y. S. Lee, "Terahertz imaging and spectroscopy of large-area single-layer graphene," *Opt. Exp.*, vol. 19, no. 1, pp. 141–146, Jan. 2011, doi: 10.1364/OE.19.000141.

[11] H.-J. Lee, E. Kim, J.-G. Yook, and J. Jung, "Intrinsic characteristics of transmission line of graphenes at microwave frequencies," *Appl. Phys. Lett.*, vol. 100, no. 22, May 2012, Art. no. 223102, doi: 10.1063/1.4722585.

[12] S. A. Awan, A. Lombardo, A. Colli, G. Privitera, T. S. Kulmala, J. M. Kivioja, M. Koshino, and A. C. Ferrari, "Transport conductivity of graphene at RF and microwave frequencies," *2D Mater.*, vol. 3, Feb. 2016, Art. no. 015010, doi: 10.17863/CAM.30788.

[13] H. S. Skulason, H. V. Nguyen, A. Guermoune, V. Sridharan, M. Siaj, C. Caloz, and T. Szkopek, "110 GHz measurement of large-area graphene integrated in low-loss microwave structures," *Appl. Phys. Lett.*, vol. 99, no. 15, Oct. 2011, Art. no. 153504, doi: 10.1063/1.3650710.

[14] D. W. Yue, C. H. Ra, X. C. Liu, D. Y. Lee, and W. J. Yoo, "Edge contacts of graphene formed by using a controlled plasma treatment," *Nanoscale*, vol. 7, no. 2, pp. 825–831, 2015, doi: 10.1039/C4NR05725B.

[15] W. R. Eisenstadt and Y. Eo, "S-parameter-based IC interconnect transmission line characterization," *IEEE Trans. Compon., Hybrids, Manuf. Technol.*, vol. 15, no. 4, pp. 483–490, Apr. 1992, doi: 10.1109/33.159877.

[16] R. L. Jackson, E. R. Crandall, and M. J. Bozack, "Rough surface electrical contact resistance considering scale dependent properties and quantum effects," *J. Appl. Phys.*, vol. 117, no. 19, May 2015, Art. no. 195101, doi: 10.1063/1.4921110.

[17] L. Kogut and K. Komvopoulos, "Electrical contact resistance theory for conductive rough surfaces," *J. Appl. Phys.*, vol. 94, no. 5, pp. 3153–3162, Sep. 2003, doi: 10.1063/1.1592628.

[18] H. Yan, F. Xia, W. Zhu, M. Freitag, C. Dimitrakopoulos, A. A. Bol, G. Tulevski, and P. Avouris, "Infrared spectroscopy of wafer-scale graphene," *ACS Nano*, vol. 5, no. 12, pp. 9854–9860, Dec. 2011, doi: 10.1021/nn203506n.